Inorganic Chemistry
Article

Inorg. Chem. **2011**, *50*, 1581–1591 **1581**
DOI: 10.1021/ic1002868

Luminescent Ruthenium Tripod Complexes: Properties in Solution and on Conductive Surfaces

Srinidhi Ramachandra,[†] Klaus C. Schuermann,[‡] Fabio Edafe,[§] Peter Belser,[§] Christian A. Nijhuis,[⊥] William F. Reus,[⊥] George M. Whitesides,[⊥] and Luisa De Cola*[,†,‡]

[†]*Laboratory of Supramolecular Chemistry and Technology, University of Twente, P.O. Box 217, 7500 AE Enschede, The Netherlands,* [‡]*Physikalisches Institut, Westfälische Wilhelms-Universität Münster, Mendelstrasse 7, 48149 Münster, Germany,* [§]*Department of Chemistry, University of Fribourg, Chemin du Musée 9, 1700 Fribourg, Switzerland, and* [⊥]*Department of Chemistry and Chemical Biology, Harvard University, 12 Oxford Street, Cambridge, Massachusetts 02138, United States*

Received February 10, 2010

Two luminescent ruthenium complexes containing tripod-type end groups linked through a rigid spacer to a phenanthroline derivative, able to confer an axial geometry to the complexes, are described. One of the compounds is functionalized with thioacetate groups in order to link the metal complex to metallic surfaces. The photophysical and electrochemical behavior of the complexes are studied in solution and on conductive substrates and, furthermore, self-assembled monolayers are investigated in a junction using gold and an indium gallium eutectic, as electrodes, and by time-resolved confocal microscopy. The results show that the complexes form very stable and well-ordered monolayers because of the tripod system, which can anchor the complex almost perpendicular to the surfaces.

Introduction

In the last decades, a large number of papers dealing with various types of molecular assemblies on metallic and semiconductor surfaces have been published because the anchoring of molecules on surfaces is the first step toward the creation of molecular devices.[1] In particular, stable electro- and photoactive species possessing a thiol derivative have been investigated to understand the role played by the chemical structures in important phenomena such as charge injection and conductivity in the general context of molecular electronics.[2] Even though most of the investigated systems are organic molecules, more recently some effort has been concentrated in the use of metal complexes containing ruthenium, iridium, and osmium ions coordinated to polypyridyl derivatives and their assemblies on conductive surfaces.[3] The advantages of using these molecules rely on their rich, often reversible, electrochemical properties, which are often localized on the metal ion, for oxidation processes, and on the ligands, for the reduction processes, on their photophysical properties, and, in particular, on the nature of their emitting excited state (triplet) and, as a consequence, long-lived excited-state lifetimes. Most of the complexes also exhibit good emission quantum yield, for

*To whom correspondence should be addressed. E-mail: decola@uni-muenster.de.

(1) (a) Love, J. C.; Estroff, L. A.; Kriebel, J. K.; Nuzzo, R. G.; Whitesides, G. M. *Chem. Rev.* **2005**, *105*, 1103–1170. (b) Dong, T. Y.; Huang, C. L.; Chen, C. P.; Lin, M. C. *J. Organomet. Chem.* **2007**, *692*, 5147–5155. (c) Ulman, A. *Chem. Rev.* **1996**, *96*, 1533–1554.

(2) (a) Mativetsky, J. M.; Pace, G.; Elbing, M.; Rampi, M. A.; Mayor, M.; Samori, P. *J. Am. Chem. Soc.* **2008**, *130*, 9192–9193. (b) Reichert, J.; Ochs, R.; Beckmann, D.; Weber, H. B.; Mayor, M.; Löhneysen, H. v. *Phys. Rev. Lett.* **2002**, *88*, 176804–176807. (c) Aviram, A.; Ratner, M. A. *Chem. Phys. Lett.* **1974**, *29*, 277–283. (d) Mirkin, C. A.; Ratner, M. A. *Annu. Rev. Phys. Chem.* **1992**, *43*, 719–754. (e) Dichtel, W. R.; Heath, J. R.; Fraser Stoddart, J. *Philos. Trans. R. Soc., A* **2007**, *365*, 1607–1625. (f) Joachim, C.; Gimzewski, J. K.; Aviram, A. *Nature* **2000**, *408*, 541. (g) Huang, Z. F.; Chen, F.; Bennett, P. A.; Tao, N. J. *J. Am. Chem. Soc.* **2007**, *129*, 13225–13231. (h) Chen, F.; Hihath, J.; Huang, Z.; Li, X.; Tao, N. J. *Annu. Rev. Phys. Chem.* **2007**, *58*, 535–564.

(3) (a) Figgemeier, E.; Constable, E. C.; Housecroft, C. E.; Zimmermann, Y. C. *Langmuir* **2004**, *20*, 9242–9248. (b) Silva, M. J. J. P.; Bertoncello, P.; Daskalakis, N. N.; Spencer, N.; Kariuki, B. M.; Unwin, P. R.; Pikramenou, Z. *Supramol. Chem.* **2007**, *19*, 115–127. (c) Bertoncello, P.; Kefalas, E. T.; Pikramenou, Z.; Unwin, P. R.; Forster, R. J. *J. Phys. Chem. B* **2006**, *110*, 10063–10069. (d) Obeng, Y. S.; Bard, A. J. *Langmuir* **1991**, *7*, 195–201. (e) Zhang, X.; Bard, A. J. *J. Phys. Chem.* **1988**, *92*, 5566–5569. (f) Meyer, T. J.; Meyer, G. J.; Pfennig, B. W.; Schoonover, J. R.; Timpson, C. J.; Wall, J. F.; Kobusch, C.; Chen, X.; Peek, B. M. *Inorg. Chem.* **1994**, *33*, 3952–3964. (g) Tuccitto, N.; Torrisi, V.; Cavazzini, M.; Morotti, T.; Puntoriero, F.; Quici, S.; Campagna, S.; Licciardello, A. *ChemPhysChem* **2007**, *8*, 227–230. (h) Cattabriga, M.; Ferri, V.; Tran, E.; Galloni, P.; Rampi, M. A. *Inorg. Chim. Acta* **2007**, *360*, 1095–1101. (i) Weiss, E. A.; Kriebel, J. K.; Rampi, M. A.; Whitesides, G. M. *Phil. Trans. R. Soc., A* **2007**, *365*, 1509–1537. (j) Albrecht, T.; Guckian, A.; Ulstrup, J.; Vos, J. G. *Nano Lett.* **2005**, *5*, 1451–1455. (k) Forster, R. J.; Figgemeier, E.; Lees, A. C.; Hjelm, J.; Vos, J. G. *Langmuir* **2000**, *16*, 7867–7870. (l) Forster, R. J.; Figgemeier, E.; Loughman, P.; Lees, A.; Hjelm, J.; Vos, J. G. *Langmuir* **2000**, *16*, 7871–7875. (m) Otsuki, J.; Tokimoto, T.; Yano, Y. N. T.; Hasegawa, T.; Chen, X.; Okamoto, Y. *Chem.—Eur. J.* **2007**, *13*, 2311–2319. (n) Terada, K.; Kobayashi, K.; Haga, M.-A. *Dalton Trans.* **2008**, 4846–4854. (o) Haga, M.-A.; Kobayashi, K.; Terada, K. *Coord. Chem. Rev.* **2007**, *251*, 2688–2701. (p) Haga, M.-A.; Wang, K.; Kato, N.; Monjushiro, H. *Mol. Cryst. Liq. Cryst.* **1999**, *337*, 89–92.

Published on Web 12/31/2010

iridium even close to unity, and excellent stability.[4] In addition, most of these systems have lately been fully investigated as materials for electroluminescent devices because their luminescent excited state can be electrically populated.[5] Their properties as organized monolayers have, however, received much less attention than many organic systems. The lack of data is related to the difficulties to anchor the luminescent metal complexes in a well-organized monolayer on conductive surfaces, mainly because of their, in most cases, octahedral geometry and therefore arrangement of their chelating ligands, and to the synthetic difficulties to introduce thiol groups.

The requirements to have good coverage and control of the distance of the luminescent center from the substrate are not easy to fulfill because the large headgroup containing the metal complex must somehow match the anchoring area in order to align the molecules as rod-type systems and the need of rigid ligands, which could hold the metal complexes perpendicular to the substrates and dictate the distance, also demands a rather long synthesis. The most commonly employed ligands to bind molecules to conductive substrates, through both covalent and noncovalent interactions, include amino, thiol, and carboxylic groups as anchoring units.[6] Multisite binding is also desirable from the application point of view because the stability of these assemblies is of critical importance. Recently, few groups have reported the use of tripodal molecules in order to strongly bind chromophores to the surface and to confer a better arrangement for the molecule to stand on the substrate.[7] Following the same rationale, we have employed a rigid tripodal ligand, functionalized with thioacetyl groups at each of the three legs, coordinated to ruthenium(II) to form a luminescent complex. In this paper, we report the synthesis and photophysical characterization of tripodal complexes, with and without anchoring groups, both in solution and on the surface and, for the thioacetyl derivative, self-assembled monolayer (SAM) formation on conductive metallic substrates. We have also examined the electrochemical behavior of these assemblies in solution and as SAMs. In addition, we also report the preliminary results on the conductance measurements of the ruthenium monolayer between two electrodes using a setup containing an eutectic alloy of indium and gallium (EGaIn) as one of the electrodes and a gold surface as the other one, to demonstrate the possible application of these molecules in molecular electronics.

Experimental Section

General Procedures. Reactants. All reactions were carried out under an argon atmosphere and in oven-dried glassware. Solvents were distilled from the appropriate drying agents. The palladium catalysts were purchased from Strem. All other reagents were obtained exclusively from Fluka, Aldrich, and Acros.

Chromatography. Thin-layer chromatography was performed using aluminum sheets precoated with silica gel 60 F_{254} purchased from Merck. Preparative plates were made by using glass sheets precoated with silica gel 60 F_{254} with a layer thickness of 2 mm purchased from Merck. Column chromatography was carried out using silica gel 60, 230−400 mesh, from Chemie Brunschwig AG and a neutral aluminum oxide gel from Fluka.

NMR. ^{1}H and ^{13}C NMR spectra were obtained with a Bruker Avance DRX-360 (360.13 MHz for ^{1}H) or a Bruker Avance DRX-400 (400.13 MHz for ^{1}H and 100.62 MHz for ^{13}C) spectrometer. Chemical shifts (δ) are given in parts per million and coupling constants (J) in Hertz, using the solvent itself as an internal standard. Assignment of the ^{1}H and ^{13}C NMR signals was performed by COSY and DEPT techniques.

MS. Mass spectra were recorded either on a Vacuum Generators Micromass VG 70/70E (fast atom bombardment ionization; nitrobenzyl alcohol or dithranol AgOTf matrix of the sample) or on a HP 5988A Quadrupol (electron impact ionization, 70 eV) mass spectrometer. Electrospray ionization (ESI) and high-resolution (HR) mass spectrometry (MS) spectra were recorded on a Bruker FTMS 4.7T BioAPEXII spectrometer.

Synthesis of Ru-SAc. A new polypyridyl ligand, 2-{4-[2-(trimethylsilyl)ethynyl]phenyl}-1*H*-imidazo[4,5-*f*][1,10]phenanthroline (TMS-EPIP), its ruthenium(II) complex, $[Ru(bpy)_2TMS\text{-}EPIP]^{2+}$ (bpy = 2,2′-bipyridine), and the target system Ru-SAc have been synthesized and characterized. The corresponding compound Ru-*tert*-Bu was prepared in a way similar to that of the caltrop with thioacetate functions.

1,10-Phenanthroline-5,6-dione,[8] *cis*-$[Ru(bpy)_2Cl_2]\cdot 2H_2O$,[9] and a trithiolacetate tripod base[10] were prepared according to literature procedures. Other reagents were purchased commercially from Fluka, Aldrich, and Acros and used without further purification unless otherwise noted.

TMS-EPIP. A mixture of 1,10-phenanthroline-5,6-dione (0.53 g, 2.50 mmol), 4-[(trimethylsilyl)-ethynyl]benzaldehyde (0.71 g, 3.50 mmol), ammonium acetate (3.88 g, 50.00 mmol), and glacial acetic acid (15 mL) was refluxed for 4 h and then cooled to room temperature (298 K). It was diluted with water, and the dropwise addition of concentrated aqueous ammonia gave a yellow precipitate, which was collected, washed with water, and dried. The crude product obtained was purified by recrystallization from $CHCl_3$/MeOH (4:1, v/v) and dried. Yield: 0.71 g (72%). ^{1}H NMR [$(CD_3)_2SO$, 360 MHz]: δ 13.88 (br, 1H, NH), 9.04 (dd, 2H, H_a), 8.92 (dd, 2H, H_c), 8.30 (d, 2H, H_e), 7.84 (q, 2H, H_b), 7.71 (d, 2H, H_d), 0.27 (s, 9H, $Si(CH_3)_3$). ^{13}C NMR [$(CD_3)_2SO$, 100 MHz]: δ 149.62, 147.94, 143.70, 132.25, 130.14, 129.58, 126.22, 123.31, 122.90, 104.82, 96.10, −0.17. ESI-MS. Calcd for $C_{24}H_{20}N_4Si$: m/z 392.15. Found: m/z 393.15 $[M + H]^+$.

Ru(bpy)$_2$TMS-EPIP. A mixture of *cis*-$[Ru(bpy)_2Cl_2]\cdot 2H_2O$ (0.5 mmol, 0.260 g), TMS-EPIP (0.5 mmol, 0.196 g), EtOH (10 mL), and water (5 mL) was refluxed under argon for 2 h to give a clear red solution. After most of the EtOH solvent was removed under reduced pressure, a red precipitate was obtained by the dropwise addition of a saturated aqueous NH_4PF_6 solution. The product was purified by column chromatography on alumina using acetonitrile/toluene (1:1, v/v) as the eluent and then dried in vacuo. Yield: 0.345 g (63%). ^{1}H NMR [$(CD_3)_2SO$, 400 MHz]: δ 14.41 (br, 1H, NH), 9.09 (dd, 2H, H_c), 8.88 (d, 2H, H_3), 8.84 (d, 2H, $H_{3'}$), 8.33 (d, 2H, H_e), 8.22 (t, 2H, H_4), 8.11 (t, 2H, $H_{4'}$),

(4) Aldachi, C. B., M. A.; Forrest, M. R.; Thompson, M. E. *Appl. Phys. Lett*. **2000**, *77*, 904–906.
(5) Yersin, H. *Highly Efficient OLEDs with Phosphorescent Materials*; Wiley-VCH Verlag GmbH & Co. KGaA: Weinheim, Germany, 2008; p 438.
(6) (a) Fox, M. A.; Whitesell, J. K.; McKerrow, A. J. *Langmuir* **1998**, *14*, 816–820. (b) Kitagawa, T.; Idomoto, Y.; Matsubara, H.; Hobara, D.; Kakiuchi, T.; Okazaki, T.; Komatsu, K. *J. Org. Chem*. **2006**, *71*, 1362–1369. (c) Park, J. S.; Vo, A. N.; Barriet, D.; Shon, Y. S.; Lee, T. R. *Langmuir* **2005**, *21*, 2902–2911.
(7) (a) Myahkostupov, M.; Piotrowiak, P.; Wang, D.; Galoppini, E. *J. Phys. Chem. C* **2007**, *111*, 2827–2829. (b) Galoppini, E.; Guo, W.; Zhang, W.; Hoertz, P. G.; Qu, P.; Meyer, G. J. *J. Am. Chem. Soc*. **2002**, *124*, 7801–7811. (c) Hoertz, P. G.; Carlisle, R. A.; Meyer, G. J.; Wang, D.; Piotrowiak, P.; Galoppini, E. *Nano Lett*. **2003**, *3*, 325–330. (d) Nikitin, K.; Lestini, E.; Lazzari, M.; Altobello, S.; Fitzmaurice, D. *Langmuir* **2007**, *23*, 12147–12153. (e) Ichimura, A. S.; Lew, W.; Allara, D. L. *Langmuir* **2008**, *24*, 2487–2493. (f) Weidner, T.; Kramer, A.; Bruhn, C.; Zharnikov, M.; Shaporenko, A.; Siemeling, U.; Trager, F. *Dalton Trans*. **2006**, 2767–2777.
(8) Amouyal, E.; Homsi, A.; Chambron, J.-C.; Sauvage, J.-P. *Dalton Trans*. **1990**, 1841–1845.
(9) Lay, P. A.; Sargeson, A. M.; Taube, H.; Chou, M. H.; Creutz, C. In *Inorganic Syntheses*; Jean'ne, M. S., Ed.; 2007; Vol. *28*, pp 291−299.
(10) Jian, H.; Tour, J. M. *J. Org. Chem*. **2003**, *68*, 5091–5103.

8.07 (dd, 2H, H_a), 7.94 (q, 2H, H_b), 7.85 (d, 2H, H_6), 7.76 (d, 2H, H_d), 7.6 (m, 4H, $H_{6'}$ and H_5), 7.35 (t, 2H, $H_{5'}$), 0.28 (s, 9H, $Si(CH_3)_3$). ^{13}C NMR [$(CD_3)_2SO$, 100 MHz]: δ 156.76, 156.55, 151.43, 151.35, 149.87, 145.11, 137.93, 137.78, 132.44, 130.42, 128.86, 128.16, 127.85, 127.71, 126.62, 126.33, 125.27, 124.43, 124.34, 123.63, 104.62, 96.57, −0.17. ESI-MS. Calcd for $C_{44}H_{36}F_{12}N_8P_2RuSi$: m/z 1096.12. Found: m/z 805.18 $[M - 2PF_6 + e^-]^+$, 951.15 $[M - PF_6]^+$.

Ru(bpy)$_2$EPIP. To a stirring solution of $[Ru(bpy)_2TMS\text{-}EPIP](PF_6)_2$ (0.164 mmol, 0.180 g) in tetrahydrofuran (THF; 10 mL) was added at room temperature a solution of K_2CO_3 (0.5−1 equiv, 12 mg) in MeOH (10 mL). After the reaction mixture was stirred at room temperature for 4 h, it was filtered and the solvent was removed in vacuo. A red precipitate was obtained by dropwise addition of a saturated aqueous NH_4PF_6 solution. The product was purified by column chromatography on alumina using acetonitrile/toluene (1:1, v/v) as the eluent and then dried in vacuo. Yield: 0.143 g (85%). ^1H NMR [$(CD_3)_2SO$, 400 MHz]: δ 14.45 (br, 1H, NH), 9.09 (d, 2H, H_c), 8.88 (d, 2H, H_3), 8.85 (d, 2H, $H_{3'}$), 8.33 (d, 2H, H_e), 8.22 (t, 2H, H_4), 8.10 (m, 4H, $H_{4'} + H_a$), 7.93 (q, 2H, H_b), 7.85 (d, 2H, H_6), 7.77 (d, 2H, H_d), 7.60 (m, 4H, $H_{6'}$ and H_5), 7.35 (t, 2H, $H_{5'}$), 4.43 (s, 1H, acetylenic). ^{13}C NMR [$(CD_3)_2SO$, 100 MHz]: δ 156.78, 156.57, 151.47, 151.39, 149.91, 145.14, 137.96, 137.81, 132.57, 130.46, 129.82, 127.89, 127.75, 126.69, 126.36, 124.46, 124.38, 123.31, 83.07, 82.94, 30.69. ESI-MS. Calcd for $C_{41}H_{28}F_{12}N_8P_2Ru$: m/z 1024.08. Found: m/z 733.14 $[M - 2PF_6 + e^-]^+$, 879.11 $[M - PF_6]^+$.

Ru-SAc. An oven-dried screw-cap tube was charged with a trithiolacetate tripod base (0.146 mmol, 0.150 g), palladium catalyst $Pd(dba)_2$ [dba = bis(dibenzylideneacetone)palladium; 3−5 mol %, 4.9 mg], CuI (3−5 mol %, 1.2 mg), and PPh_3 (12−20 mol %, 7.7 mg). The tube was capped with a septum, evacuated, and backfilled with argon three times. Triethylamine (5 mL) was added via a syringe. A solution of $[Ru(bpy)_2EPIP](PF_6)_2$ (0.146 mmol, 0.150 g) in THF (5 mL) was transferred via a cannula to the tube. The tube was then capped with its screw cap, and the solution was stirred at room temperature for 3 days. After most of the solvent was removed under reduced pressure, an orange precipitate was obtained by the dropwise addition of a saturated aqueous NH_4PF_6 solution. The product was purified by column chromatography on silica, eluting with a gradient of acetonitrile/water/saturated aqueous KNO_3 from 100:1:1 to 100:18:2. The collected orange fractions were combined and dissolved in acetone. An aqueous solution of saturated ammonium hexafluorophosphate was added, and acetone was evaporated. Filtration under vacuum and washing with H_2O of the resulting precipitate afforded the desired caltrop (0.18 g, 64%) as an orange solid. ^1H NMR [CD_2Cl_2, 400 MHz]: δ 9.16 (d, 2H), 8.47 (d, 2H,), 8.43 (d, 2H), 8.33 (d, 2H), 8.11 (t, 2H), 7.80 (t, 2H), 7.93 (d, 2H), 7.80 (m, 6H), 7.70 (d, 2H), 7.60 (m, 16H), 7.51 (m, 5H), 7.43 (m, 3H), 7.30 (m, 8H), 4.11 (s, 6H), 2.35 (s, 9H). ESI-MS. Calcd for $C_{98}H_{70}F_{12}N_8O_3P_2RuS_3Si$: m/z 1922.28. Found: m/z 816.18 $([M - 2PF_6]^{2+})/2$.

Synthesis of Ru-*tert*-Bu. Ethoxytris[4-(4-*tert*-butylphenylethynyl)phenyl]silane (Ethoxy-*tert*-Bu). To an oven-dried glass vessel containing 4-*tert*-butylphenylacetylene (2.4 mL, 13.2 mmol), ethoxytris(*p*-iodophenyl)silane (1.53 g, 2.2 mmol), $Pd(dba)_2$ (0.19 g, 0.33 mmol), copper iodide (0.06 g, 0.3 mmol), and triphenylphosphine (0.29 g, 1.1 mmol) were added 150 mL of THF and 50 mL of triethylamine, which was filled with argon. The mixture was stirred at room temperature for 2 days. The reaction mixture was then poured into water, and the aqueous layer was extracted with ethyl acetate three times. The combined organic solution was washed with water and dried over magnesium sulfate. The solvent was removed in vacuo, and the residues were purified by column chromatography on silica gel (hexanes/CH_2Cl_2, 5:1) to give ethoxy-*tert*-Bu as a yellow sticky oil (1.65 g, 95%). ^1H NMR (CD_2Cl_2, 400 MHz): δ 7.58−7.47 (m, 12H), 7.48 (d, 6H, J = 8.4), 7.38 (d, 6H, J = 8.4), 3.89 (q, 2H, J = 7.0), 1.33 (s, 27H), 1.26 (t, 3H, J = 7.1). ^{13}C NMR (CD_2Cl_2, 100 MHz): δ 151.9, 135.3, 134.0, 131.6, 131.0, 125.5, 120.2, 91.0, 60.1, 35.0, 31.3, 18.6. MALDI-MS (matrix = DCTB). Calcd for $C_{56}H_{56}IOSi$: m/z 772.41. Found: m/z 772.42.

Tris[4-(4-*tert*-butylphenylethynyl)phenyl]-4′-iodophenylsilane (Iodophenyl-*tert*-Bu). A solution of $Li[C_6H_4I]$ was prepared first by the addition of 1.6 M $LiBu^n$ in hexane (8.9 mL, 1.11 equiv) to *p*-diiodobenzene (0.495 g, 1.5 mmol) in diethyl ether (10 mL) and stirred for 1 h at room temperature under argon. The resulting solution was transferred dropwise to a solution of ethoxy-*tert*-Bu (1.00 g, 1.28 mmol) in 20 mL of dry pentane. The resulting mixture was stirred at room temperature overnight and then poured into H_2O, and the mixture was extracted with CH_2Cl_2. The combined organic layer was dried over $MgSO_4$ and filtered, and the solvent was removed in vacuo. The residue was purified by column chromatography to afford a slightly yellow clear oil (0.655 g, 55%). ^1H NMR (CD_2Cl_2, 400 MHz): δ 7.79 (d, 2H, J = 8.1), 7.57−7.7.52 (m, 12H), 7.48 (d, 6H, J = 8.2), 7.41 (d, 6H, J = 8.4), 7.30 (d, 2H, J = 8.2), 1.33 (s, 27H). ^{13}C NMR (CD_2Cl_2, 100 MHz): δ 152.60, 138.43, 137.79, 136.75, 133.74, 133.37, 131.87, 131.47, 126.05, 125.68, 120.42, 97.92, 91.45, 88.94, 35.28, 31.44. MALDI-MS (matrix = DCTB). Calcd for $C_{60}H_{55}OSi$: m/z 930.31. Found: m/z 930.32.

[Ru(bpy)$_2$EPIP](PF$_6$)$_2$-Si-Tripod-*tert*-Bu] (Ru-*tert*-Bu). An oven-dried screw-cap tube was charged with tripod-*tert*-Bu (0.150 g, 0.146 mmol), palladium catalyst bis(dibenzylideneacetone)palladium(0) (5.6 mg, 0.01 mmol), CuI (1.9 mg, 0.01 mmol), and PPh_3 (10.3 mg, 0.039 mmol). The tube was capped with a septum, evacuated, and backfilled with argon three times. *N*, *N*-Diisopropylethylamine (5 mL) was added via a syringe. A solution of $[Ru(bpy)_2EPIP](PF_6)_2$ (200 mg, 0.195 mmol) in THF (5 mL) was transferred via a cannula to the tube. The tube was then capped with its screw cap, and the solution was stirred at room temperature for 2 days. The solvent was removed under reduced pressure to give a solid residue, which was dissolved in water (10 mL), NH_4PF_6 (0.5 g) was added, and the resulting red precipitate was isolated by suction filtration. The red precipitate was first purified by column chromatography on alumina (1:1 acetonitrile/toluene) to remove the unreacted tripod-OMe and then eluted with a gradient of acetonitrile/water/saturated aqueous KNO_3 from 100:1:1 to 100:18:2. The collected orange fractions were combined and evaporated. An aqueous solution of saturated ammonium hexafluorophosphate was added. Filtration under vacuum with Celite, washing with H_2O, and dissolution in acetone afforded the desired Ru-tripod as a red powder. Yield: 0.148 g (45%). ^1H NMR (DMSO-d_6, 400 MHz): δ 14.55 (br, 1H), 9.12 (d, 2H, J = 8.1), 8.85 (d, 2H, J = 8.3), 8.81 (d, 2H, J = 8.1), 8.39 (d, 2H, J = 8.3), 8.21 (t, 2H, J = 7.8), 8.12−8.06 (m, 2H), 7.88 (d, 2H, J = 8.6), 7.84 (d, 2H, J = 5.0), 7.71 (d, 2H, J = 8.1), 7.67−7.45 (m, 34H), 7.34 (d, 2H, J = 6), 1.29 (s, 27H).

HR ESI-MS. Calcd for $C_{101}H_{82}N_8RuSi$: m/z 768.27454. Found: m/z 768.27429 $([M - 2PF_6]^{2+}/2)$.

^{13}C NMR (CD_3CN, 500 MHz): δ138.77, 137.43, 137.35, 135.38, 134.45, 133.44, 133.12, 133.09, 132.80, 132.72, 132.35, 132.13, 131.97, 131.66, 130.40, 129.79, 129.70, 128.62, 128.48, 127.86, 127.14, 126.77, 126.08, 125.81, 125.41, 125.31, 125.23, 120.76, 92.20, 91.86, 91.03, 89.25, 31.40.

Photophysics. Absorption spectra were measured on a Varian Cary 5000 double-beam UV−vis−near-IR (NIR) spectrometer and baseline-corrected. Steady-state emission spectra were recorded on a Horiba Jobin-Yvon IBH FL-322 Fluorolog 3 spectrometer equipped with a 450 W xenon arc lamp, double-grating excitation and emission monochromators (2.1 nm/mm dispersion; 1200 grooves mm^{-1}), and a Hamamatsu R928 photomultiplier tube or a TBX-4-X single-photon-counting detector. Emission spectra were corrected for the source intensity (lamp and grating) and emission spectral response (detector and grating) by standard

correction curves. For monolayers, the sample was mounted on a commercially available solid-state sample holder provided by Horiba Jobin-Yvon, and the emission was collected with the front-face geometry. Time-resolved measurements were performed using the time-correlated single-photon-counting option on the Fluorolog 3. NanoLEDs [402 nm; full width at half-maximum (fwhm) < 750 ps] with repetition rates between 10 kHz and 1 MHz were used to excite the sample. The excitation sources were mounted directly on the sample chamber at 90° to a double-grating emission monochromator (2.1 nm/mm dispersion; 1200 grooves mm^{-1}) and collected by a TBX-4-X single-photon-counting detector. The photons collected at the detector are correlated by a time-to-amplitude converter (TAC) to the excitation pulse. Signals were collected using an IBH DataStation Hub photon-counting module, and data analysis was performed using the commercially available *DAS6* software (Horiba Jobin Yvon IBH). The goodness of fit was assessed by minimization of the reduced χ^2 function and visual inspection of the weighted residuals.

Quantum Yield. Luminescence quantum yields (Φ_{em}) were measured in optically dilute solutions (O.D. < 0.1 at excitation wavelength) and compared to reference emitters by the following equation:

$$\Phi_x = \Phi_r \left[\frac{A_r(\lambda_r)}{A_x(\lambda_x)}\right]\left[\frac{I_r(\lambda_r)}{I_x(\lambda_x)}\right]\left[\frac{{n_x}^2}{{n_r}^2}\right]\left[\frac{D_x}{D_r}\right]$$

where A is the absorbance at the excitation wavelength (λ), I is the intensity of the excitation light at the excitation wavelength (λ), n is the refractive index of the solvent, D is the integrated intensity of the luminescence, and Φ is the quantum yield. The subscripts r and x refer to the reference and sample, respectively. All quantum yields were performed at identical excitation wavelengths for the sample and reference, canceling the $I(\lambda_r)/I(\lambda_x)$ term in the equation. The quantum yield of the reference compound, $Ru(bpy)_3$, was obtained from the literature ($\Phi = 0.016$).[11] Deaerated samples were prepared by the freeze−pump−thaw technique.

Cyclic Voltammetry (CV). CV was performed in a gastight single-compartment three-electrode cell using a Voltalab 40 system from Radiometer Analytical that consists of a PGZ301 potentiostat and *Voltamaster 4* software. The working electrode was a 1 mm platinum disk, the counter electrode was a platinum wire, and silver wire was used as a pseudoreference electrode. All glassware was dried prior to use. The compounds (electrolyte, analyte, and reference) were placed in a Schlenk flask, which was then evacuated and heated with a heat gun to eliminate any moisture and oxygen that had entered during the addition. The flask was then evacuated and filled three times with dry N_2(g). The solvent was added via syringe directly to the sealed Schlenk flask and then degassed for 10 min with a gentle stream of dry N_2. After degassing, the solution was added, via a syringe, to the electrochemical cell under a positive N_2 pressure and the electrodes were then added. The solution was kept under a positive N_2 pressure during the measurements, but no flow was allowed through the cell. For electrochemistry of the surfaces, silver and platinum wires were used as reference and counter electrodes, respectively. The reason for employing the platinum electrode was the fact that the electrochemical window of gold is not large enough for the ruthenium complex. The surface coverage on platinum is presented in the Supporting Information. Subsequent experiments were carried out using a neat acetonitrile solution with tetrabutylammonium hexafluorophosphate ($TBAPF_6$; Sigma Aldrich) as the electrolyte (0.1 M). Measurements with both gold and indium/tin oxide (ITO) functionalized with Ru-SAc were performed in the same experimental conditions as mentioned above.

(11) Issberner, J.; Vogtle, F.; De Cola, L.; Balzani, V. *Chem.—Eur. J.* **1997**, *3*, 706.

Surface Analysis. Atomic Force Microscopy (AFM) Imaging. AFM images of the monolayers on flat gold substrates were acquired in air at room temperature with a commercial instrument (Digital Instruments, Nanoscope IIIa, Dimension 3000, Santa Barbara, CA) operating in tapping mode. AFM images are flattened and shown without further modification. Analysis was performed using WSxM 4.0 Develop.[12]

Fluorescence Lifetime Microscopy (FLIM). FLIM images and the fluorescence decays on surfaces were recorded using a Microtime 200 (PicoQuant) attached to an Olympus IX 71 microscope with a 100× oil-immersion objective and a scanning speed of 6 μs per point at excitation with a 440 nm laser (fwhm 80 ps). Fluorescent lifetimes were calculated from the whole area by the software *SymphoTime* (PicoQuant).

Formation of the Junctions. Ultraflat gold surfaces were formed by a template-stripping (TS) procedure published previously.[13] All of the details can be found in ref 14, but a brief description is given here. On silicon wafers with their native SiO_2 layer present, a layer of 500 nm of gold was thermally deposited by electron beam (e-beam) at $(2-3) \times 10^{-6}$ Torr at a rate of 8−10 Å s^{-1}. Glass slides, which were cleaned by washing with EtOH and by a plasma of air (500 Torr, 5 min), of typically 1 cm^2 were glued at the silver surface using an optical adhesive (Norland, No. 61). The optical adhesive was cured by exposure to UV light for 2 h. The glass substrates were cleaved off the silicon wafer by using a razor blade, after which the TS gold substrates were immersed in a solution of 2 mM Ru-SAc in EtOH/acetonitrile for 24 h at room temperature. After SAM formation, the samples were rinsed with EtOH.

Conical-shaped EGaIn alloy (75.5% gallium and 24.5% indium by weight, 15.7 °C melting point, with a surface layer of Ga_2O_3) was used as the top electrode. A detailed description of the formation and contact of the SAMs by Ga_2O_3/EGaIn top electrodes has been reported previously.[15,16] Ga_2O_3/EGaIn is a non-Newtonian fluid. On the micrometer scale, Ga_2O_3/EGaIn behaves as a solid, but when sheer pressure is applied, Ga_2O_3/EGaIn behaves as a liquid. Ga_2O_3/EGaIn will flow until the sheer pressure is relieved. This behavior, unlike mercury, allows one to shape Ga_2O_3/EGaIn into nonspherical shapes. A drop of Ga_2O_3/EGaIn hanging at a 26S-guage needle was brought into contact with a surface that is wettable by Ga_2O_3/EGaIn, such as poly(dimethylsiloxane), glass, or silver surfaces. Ga_2O_3/EGaIn adheres both to the surface and to the needle. Slowly retracting the needle from the EGaIn drop, by using a micromanipulator, deforms the EGaIn drop in such a way that two conical-shaped Ga_2O_3/EGaIn structures connected head-to-head arise. Further retraction of the needle results in separation of the conical-shaped Ga_2O_3/EGaIn structures, one at the needle and one at the surface. Subsequently, the substrate was discarded and replaced by a TS silver surface with the SAM of interest, and the conical-shaped Ga_2O_3/EGaIn at the needle was brought into contact with the SAM.

Results and Discussion

All of the ligands and ruthenium(II) complexes as well as their abbreviations are shown in Scheme 1.

Synthesis of the Trithiolacetate Tripod Base. This molecular base with thiol anchoring groups is prepared in the same way as that described by Jian and Tour[10] with a

(12) Horcas, I.; Fernandez, R.; Gomez-Rodriguez, J. M.; Colchero, J.; Gomez-Herrero, J.; Baro, A. M. *Rev. Sci. Instrum.* **2007**, *78*, 013705–8.

(13) Weiss, E. A.; Kaufman, G. K.; Kriebel, J. K.; Li, Z.; Schalek, R.; Whitesides, G. M. *Langmuir* **2007**, *23*, 9686–9694.

(14) Weiss, E. A.; Chiechi, R. C.; Kaufman, G. K.; Kriebel, J. K.; Li, Z.; Duati, M.; Rampi, M. A.; Whitesides, G. M. *J. Am. Chem. Soc.* **2007**, *129*, 4336–4349.

(15) Chiechi, R. C.; Weiss, E. A.; Dickey, M. D.; Whitesides, G. M. *Angew. Chem., Int. Ed.* **2008**, *47*, 142–144.

(16) Nijhuis, C. A.; Reus, W. F.; Whitesides, G. M. *J. Am. Chem. Soc.* **2009**, *131*, 17814–17827.

Scheme 1. Schematic Formulas of All of the Complexes Investigated and Their Precursors[a]

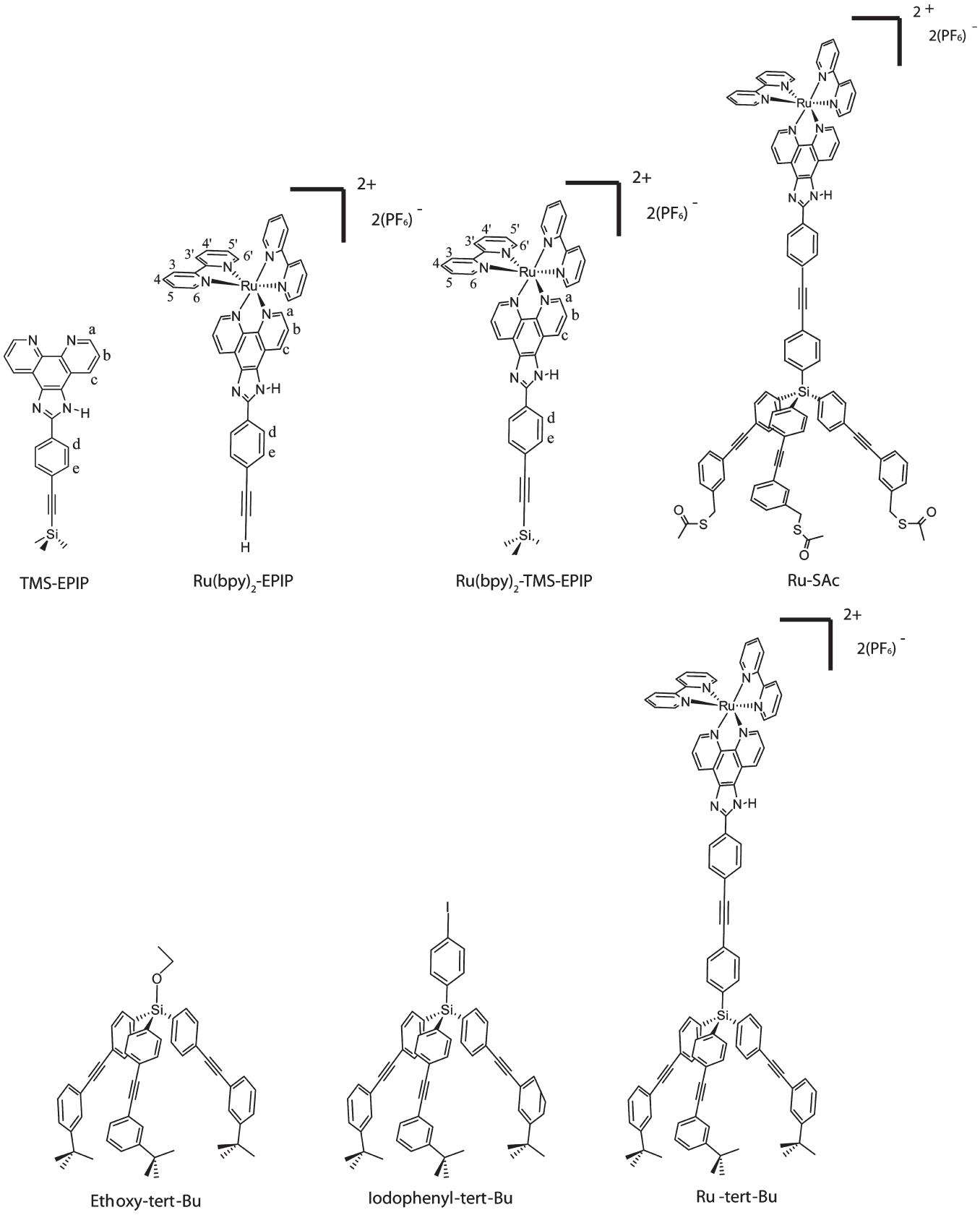

[a] The molecules will be named with the abbreviation shown under each formula.

modification in the preparation of the tris[4-[3-(*tert*-butyldimethylsilanyloxymethyl)phenylethynyl]phenyl]-4′-iodophenylsilane in which dry pentane was used as the solvent instead of THF.

Synthesis of the *tert*-Butyl Tripod Base. The construction of the molecular base without anchoring groups starts with the synthesis of ethoxytris(*p*-iodophenyl)silane[17] followed by a Sonogashira coupling reaction of this molecule with 3 equiv of 4-*tert*-butylphenylacetylene. The desired molecule is afforded by lithiation of 1,4-diiodobenzene and the addition of 4-iodophenyllithium to ethoxytris-[4-(4-*tert*-butylphenylethynyl)phenyl]silane.

A previous description of the synthesis of a similar tripod base in the literature[10] mentioned some problems during the addition of 4-iodophenyllithium (prepared in situ in dry ether) to ethoxytris[4-[3-(TBDMSO)phenylethynyl)phenyl]silane (dissolved in dry THF) or also by the reverse addition (TBDMSO = *tert*-butyldimethylsilyloxy). The preparation of tris[4-[(3-(TBDMSO)methyl)-phenylethynyl]phenyl]-4′-iodophenylsilane as described[10] gave a very poor yield, which is far from the predicted 88% yield. Finally, we solved that problem by using dry pentane as the solvent in the reaction between 4-iodophenyllithium and ethoxytris[4-(4-*tert*-buylphenylethynyl)phenyl]silane. Under such conditions, we got an acceptable yield of roughly 50%.

Synthesis of Ruthenium(II) Complexes. Ruthenium(II) complexes containing the TMS-EPIP ligand were prepared by the direct reaction of yellow TMS-EPIP with the appropriate mole ratios of the purple $Ru(bpy)_2Cl_2$ in MeOH/water for 2 h. The desired orange ruthenium(II) complex was isolated as its hexafluorophosphate and was purified by column chromatography. $[Ru(bpy)_2EPIP](PF_6)_2$ was obtained by removal of the trimethylsilyl protecting group from $[Ru(bpy)_2TMS\text{-}EPIP](PF_6)_2$ with K_2CO_3 in MeOH. The Ru-SAc and Ru-*tert*-Bu complexes have been synthesized by a Sonogashira cross-coupling reaction between $[Ru(bpy)_2EPIP](PF_6)_2$ and respectively the trithiolacetate tripod base[10] or *tert*-butyl tripod base in the presence of $Pd(dba)_2$ palladium catalysts [$Pd(dba)_2$ = bis(dibenzylideneacetone)palladium(0)]. See the Experimental Section for the preparation of all of the precursors and the full characterization of the molecules.

Photophysical Characterization in Solution. The absorption spectrum of Ru-SAc in an acetonitrile solution is shown in Figure 1. The high-energy band at 291 nm (ε = 1.08×10^5 M^{-1} cm^{-1}) can be assigned to the bipyridine and phenanthroline singlet intraligand (^{1}IL) $\pi-\pi^*$ transitions, while the bands at 312 nm (ε = 8.1×10^4 M^{-1} cm^{-1}) and 341 nm (ε = 3.7×10^4 M^{-1} cm^{-1}) are due to the $\pi-\pi^*$ absorptions of the highly conjugated moieties containing the phenyleneethylene groups. In particular, the lowest-energy band is due to 2-[4-(2-ethynyl)phenyl]-1*H*-imidazo[4,5-*f*][1,10]phenanthroline,[18] while the 312 nm feature is attributed to the tripod species. This assignment is corroborated by the observation that, for the two reference non-tripodal complexes $Ru(bpy)_2EPIP$ and $Ru(bpy)_2TMS\text{-}EPIP$, this 312 nm band is missing (see Figure 1). The lowest-energy bands around 458 nm (ε = 1.5×10^4 M^{-1} cm^{-1}) are assigned to singlet metal-to-ligand charge-transfer (^{1}MLCT) transitions, which are typical for ruthenium polypyridyl complexes, involving the d orbitals of the ruthenium and the π^* orbitals of the bipyridine and phenanthroline ligands.

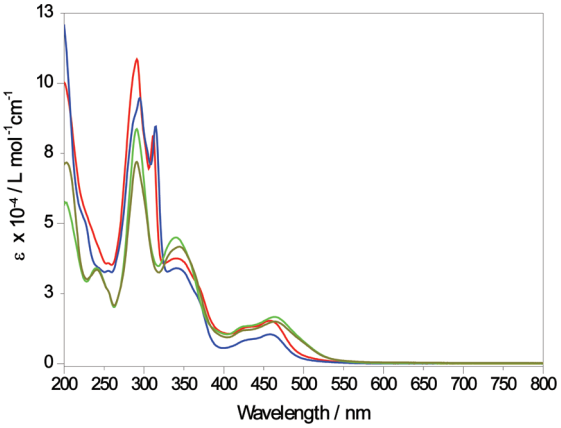

Figure 1. Absorption spectra of Ru-SAc (red line), Ru-*tert*-Bu (blue line), $Ru(bpy)_2EPIP$ (green line), and $Ru(bpy)_2TMS\text{-}EPIP$ (red line) in acetonitrile solutions.

Because of the similar energy levels involving the bipyridine and phenanthroline ligands and the broadness of the spectra, it is difficult to attribute the lowest excited state from the absorption characteristics. We can therefore expect that for complexes containing the tripod with thioacetate and *tert*-butyl groups the lowest MLCT involves the bipyridine ligands or the substituted phenanthroline. On the other hand, for $Ru(bpy)_2EPIP$ and $Ru(bpy)_2TMS\text{-}EPIP$, because of higher conjugation and the lack of electron-donating groups, we expect the lowest MLCT absorption on the phenanthroline moiety. Such a hypothesis is supported by the emission spectra and electrochemistry data of the complexes.

The room temperature emission spectra of the reference compound, Ru-*tert*-Bu, and the Ru-SAc complex were recorded in acetonitrile solutions upon excitation at 452 nm (Figure 2a). The emission spectra have broad structureless bands centered at 609 and 614 nm for Ru-SAc and Ru-*tert*-Bu, respectively. These bands are attributed to the radiative decay of the triplet metal-to-ligand charge-transfer (^{3}MLCT) state of the ruthenium complexes to the ground state. The red shift of the emission band for the Ru-*tert*-Bu complex versus the Ru-SAc complex can be due to the slightly electron-donating nature of the *tert*-butyl groups, which can then increase the σ donation of phenanthroline, favoring the involvement of the bpy ligands in the ^{3}MLCT lowest excited state. The excited-state lifetimes for both complexes are very similar in acetonitrile solutions (see Table 1), and in deaerated solutions, both compounds show much longer excited-state lifetimes, as expected because of the triplet character of the lowest excited states. The emission quantum yields of the complexes were measured using the $Ru(bpy)_3^{2+}$ complex as the reference (Φ_{em} = 0.016)[11] in aerated acetonitrile, and the values are reported in Table 1. In the deaerated solutions, as expected, the emission quantum yields of the complexes are higher than those for analogous aerated complexes. The precursor complexes also emit at room temperature, and their emission spectra are quite similar to those of the other compounds. In the same solvent, they show emission maxima that are slightly red-shifted compared with those of the tripod systems, λ = 617

(17) Yao, Y.; Tour, J. M. *J. Org. Chem.* **1999**, *64*, 1968–1971.
(18) Huang, W. Y.; Gao, W.; Kwei, T. K.; Okamoto, Y. *Macromolecules* **2001**, *34*, 1570–1578.

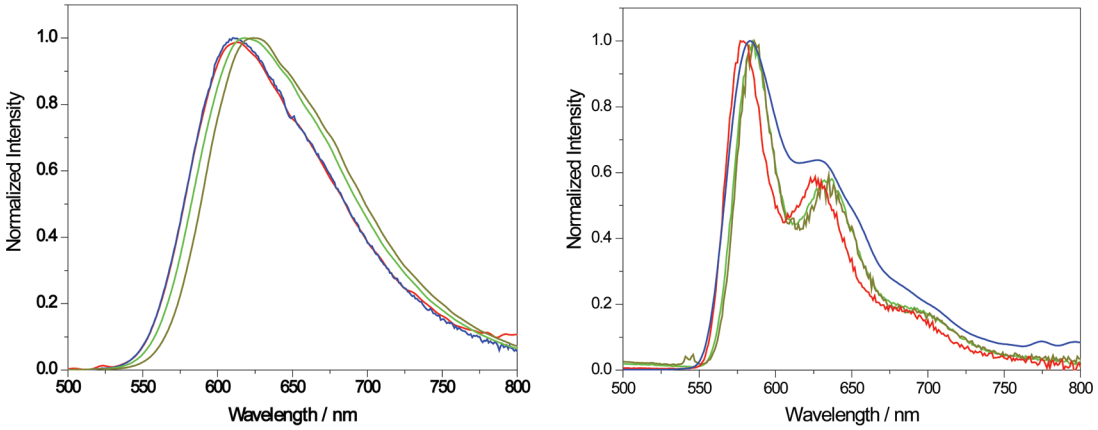

Figure 2. (a) Emission spectra of Ru-SAc (red line), Ru-*tert*-Bu (blue line), $Ru(bpy)_2EPIP$ (light-green line), and $Ru(bpy)_2TMS$-EPIP (dark-green line) in acetonitrile solutions. (b) Emission spectra measured at 77 K in butyronitrile glass. λ_{ex} = 452 nm.

Table 1. Photophysical Data in an Acetonitrile Solution, Unless Otherwise Specified, for All of the Complexes Investigated

	emission						
	room temperature					77 K	
complex	λ_{max} (nm)	ϕ^a	ϕ^b	τ (μs)^a	τ (ns)^b	λ_{max} (nm)^c	τ (μs)^c
Ru-SAc	609	0.12	0.014	1.04	155	579, 626	5.2
Ru-*tert*-Bu	614	0.14	0.018	1.14	196	580, 628	5.6
$Ru(bpy)_2EPIP$	617	0.08	0.015	1.08	178	586, 635	5.3
$Ru(bpy)_2TMS$-EPIP	621	0.10	0.020	1.05	203	585, 637	5.2
Ru-SH on gold	619			2.0	8.0		
Ru-SAc on glass	615			0.09	812		

[a] In a degassed solution. [b] In an air-equilibrated solution. [c] In butyronitrile glass. For lifetime measurements, a 402 nm laser diode was used as the excitation source. For lifetimes on gold and glass, a 440 nm laser excitation was used.

and 621 nm for $Ru(bpy)_2EPIP$ and $Ru(bpy)_2TMS$-EPIP, respectively. The 77 K emission spectra, recorded in butyronitrile glass (Figure 2b), show a blue shift relative to the room temperature solution measurements, as expected for an MLCT emission spectrum similar to what is known for ruthenium polypyridyl complexes.[19] The excited-state lifetimes at 77 K (Table 1) are longer than those at room temperature, and such behavior is attributed to the lack of thermal population of the triplet metal-centered (^{3}MC) states, which would otherwise quench the luminescent excited state.[20]

Preparation of the SAMs. In order to perform local measurements on the SAMs, the prerequisite is a surface with a very high degree of flatness. Hence, we prepared the ultraflat gold substrates on a microscope coverslip using the TS method as described by Weiss and coworkers.[14]

The samples were immediately immersed in an EtOH solution of the tripod molecules and left for 24 h for monolayer formation. A total of 10 μL of a hydrazine solution was added to deprotect the thioacetyl groups in situ to facilitate Ru-SH monolayer formation. The samples were subsequently rinsed with EtOH to remove any unbound molecules. As the AFM picture shows (Figure 3), the monolayer is not homogeneous but forms islands, which is well-known for other thiolate complexes on surfaces.[1b,3n] The same procedure was applied to the reference com-

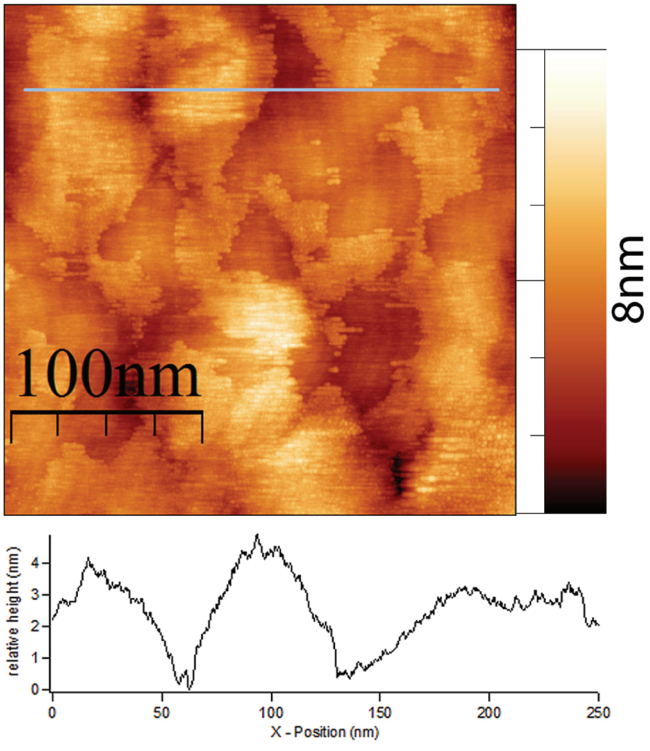

Figure 3. AFM picture of the SAM of Ru-SH on a gold substrate and a height profile, revealing the formation of islands with heights corresponding to the dimensions of the molecule.

(19) Campagna, S.; Puntoriero, F.; Nastasi, F.; Bergamini, G.; Balzani, V. Photochemistry and Photophysics of Coordination Compounds: Ruthenium. *Photochemistry and Photophysics of Coordination Compounds I*; 2007; pp 117−214.

(20) Juris, A. B. V.; Barigelletti, F.; Campagna, S.; Belser, P.; von Zelewsky, A. *Coord. Chem. Rev.* **1988**, *84*, 85–277.

pound Ru-*tert*-Bu, but no monolayer was found because the lack of anchoring groups does not allow any strong bond to the gold surface, and therefore after the first wash, the complex was rinsed away. The AFM picture indicates, however, that the islands of Ru-SAc are sufficiently large to perform local measurements and the quality and height of the layers confirm monolayer formation, their stability, and good packing, as is also indicated by the high yields in the Ga_2O_3/EGaIn measurements (vide infra). Furthermore, when a control experiment was performed, by immersion of a bare gold surface in the EtOH solution under identical conditions, it revealed no such island formation, supporting our claim that the islands are indeed due to monolayer formation. This experiment also suggested that the depth profile of about 3 nm, which is indicated by AFM, is not due to the surface roughness of the gold.

Photophysical Measurements of the Ru-SH Monolayer. The emission measurements of the Ru-SH monolayer on an ultraflat gold substrate were successfully carried out in the spectrofluorimeter, indicating that despite the quenching induced by the gold surface the signal strength from the monolayer was detectable. The emission of the monolayer (Figure 4) resembled the emission profile of Ru-SH in solution. However, we see a red shift of 4 nm in the emission with respect to the solution measurements. This could suggest that the lowest excited state involves the phenanthroline ligand, which, because of high conjugation, feels the electronic interaction with the gold surface. In other words, upon anchoring of the complexes on the substrate, the ^{3}MLCT state would be localized on the chelating 2-[4-(2-ethynyl)phenyl]-1*H*-imidazo[4,5-*f*][1,10]phenanthroline moiety and the electron-withdrawing effect of the gold substrate lowers the lowest unoccupied molecular orbital (LUMO) of the ligand, shifting the emission at lower energy. In order to clarify the effect of the binding on the gold surface, we have also drop-casted the solution on glass (Figure 4). We were also able to measure the excitation spectrum of this monolayer because the signal strength was high enough, indicating a high packing density (Figure S1 in the Supporting Information).

The excited-state lifetimes of the Ru-SH molecules after their immobilization, through binding of the thiol groups on the gold, were measured using a time-resolved confocal microscope. The lifetimes were fit to a biexponential, with a shorter component of 2 ns and a longer component of 8 ns (Figure 5). This dual-exponential decay could be due to the different orientations of the molecules on the surfaces, for instance, coordination of two out of the three thiols, leading to a different tilt angle of the ruthenium complex versus the surface upon coordination of all of the three anchoring groups. The X-ray photoelectron spectroscopy (XPS) measurements indicate that at least two out of the three groups surely are attached to the gold surface (Figure S2 in the Supporting Information), and this is consistent with what was reported for similar systems.[10] Another possible explanation for the presence of two components is triplet−triplet annihilation due to a strong packing of the complexes with a consequent quenching of the emission. In order to evaluate the extent of the quenching, we compared the film of Ru-SH by the drop cast method on a microscopy glass plate, measuring the lifetime of the ruthenium emission. The lifetime was fit to a biexponential decay even though we can also assume

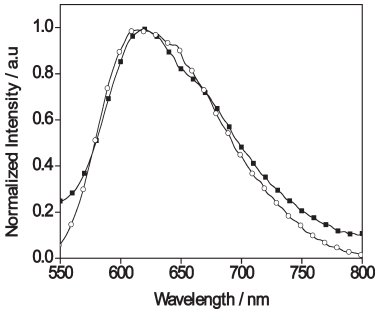

Figure 4. Emission spectra of the Ru-SH monolayer on an ultraflat gold substrate (■) and Ru-SH drop cast on glass (○).

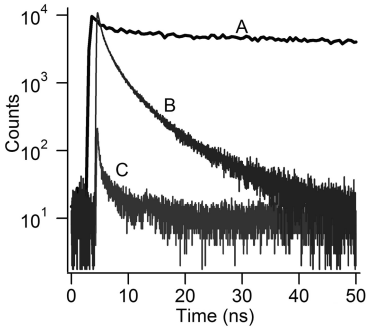

Figure 5. Decay profiles of (A) Ru-SH on glass, (B) Ru-SH on gold, (C) and bare gold. λ_{ex} = 440 nm.

almost monoexponential behavior, because of the fact that the short component has a weight of less than 10% on the entire signal. The long component has an excited-state lifetime of 812 ns and the shorter minor component of about 90 ns. This is in good agreement with the value reported for other ruthenium complexes on glass (700 ± 50 ns).[21] Because the glass cannot play any role in the quenching of the emission, we attribute the short component to a possible high local concentration of ruthenium complexes, which could lead to self-quenching. The long excited-state lifetime can be, therefore, taken as a good reference for the unquenched ruthenium complex on an inert substrate.

In the case of the SAM, we can, therefore, conclude that quenching of the emission is due to a photoinduced energy and/or electron transfer from the metal complex to the gold surface as reported earlier.[22] In particular, for similar ruthenium complexes anchored onto the gold nanocrystalline surface, it has been reported that the origin of quenching comes mainly from an electron transfer from the excited-state ruthenium complex to the gold surface.[23] The quenching rate can be calculated using the following equation and the 8 ns lifetime for Ru-SH on gold and 812 ns for Ru-SH on glass.

$$k_{eT} = \frac{1}{\tau} - \frac{1}{\tau_0}$$

The rate constant was determined to be 1.23×10^8 s^{-1}. This estimated rate constant is about 3 orders of magnitude

(21) Wei, S.; Gafney, H. D.; Clark, J. B.; Perettie, D. J. *Chem. Phys. Lett.* **1983**, *99*, 253–257.
(22) D'Aleo, A.; Williams, R. M.; Chriqui, Y.; Iyer, V. M.; Belser, P.; Vergeer, F.; Ruiz, V.; Unwin, P. R.; De Cola, L. *Open Inorg. Chem. J.* **2007**, *1*, 26–36.
(23) Pramod, P.; Sudeep, P. K.; Thomas, K. G.; Kamat, P. V. *J. Phys. Chem. B* **2006**, *110*, 20737–20741.

higher than that reported by Unwin and co-workers for a thiolated ruthenium complex on a gold surface (1×10^5 s^{-1})[3c] and about 2 orders of magnitude larger than that reported by Kamat and co-workers for electron transfer from a ruthenium complex to gold nanoparticles (1.1×10^6 s^{-1}).[23] However, in both of the above cases, they have alkyl linkers to the gold surface, which surely slow down the electron-transfer processes compared to our fully conjugated rigid tripod system.

Electrochemical Measurements. Electrochemistry of the reference compound, Ru-*tert*-Bu, as well as the thiolated Ru-SH was performed in solutions. The Ru-SH electrochemistry was compared with the results obtained on SAMs on a platinum-disk electrode. In an acetonitrile solution with $TBAPF_6$ as the supporting electrolyte, both of the complexes show reversible reduction and oxidation waves. In particular, the first oxidation occurs at +1.31 V (vs saturated calomel electrode, SCE). The peak-to-peak separation is 90 mV. The observed peak-to-peak separation is larger than the expected peak-to-peak separation for an ideal Nernstian behavior (ca. 59 mV). However, because the reference redox species ferrocene also showed this, we can attribute the observed effect to the ohmic drop in such systems; similar behavior is also reported by Bard and co-workers.[24]

The reversible oxidation can be attributed to oxidation of the ruthenium center Ru^{III}/Ru^{II} and occurs at potentials similar to that of $[Ru(bpy)_2(phen)]^{2+}$.[25] The first reduction at −1.33 V can be attributed to reduction of the bipyridine ligand.

For electrochemistry on monolayers, a 1 mm platinum-disk electrode, precleaned thoroughly by repeated sonication with deionized water and acetonitrile (spectroscopic grade), was used to form Ru-SH monolayers by immersion of this precleaned platinum electrode in a concentrated solution of Ru-SAc in acetonitrile ($\sim 10^{-3}$ M). The thioacetate groups were deprotected in situ by adding ~ 10 μL of a hydrazine solution to obtain the Ru-SH complex. The electrode was later (after 48 h of immersion) rinsed with acetonitrile before measurements to eliminate any adsorbed complex. The cyclic voltammogramms were measured with different scan rates and referenced against SCE with a silver wire as a quasi-reference electrode. Oxidation of the ruthenium ion occurs at +1.38 V, very similar to the value obtained in solution. It is interesting to note that the peak separation ΔE_p is greater than 0 and increases with increasing scan rates (210 mV at 1000 mV s^{-1} compared to 52 mV at 100 mV s^{-1}; see Figure 6). This is consistent with similar trends observed for osmium bipyridine complexes on gold surfaces.[26] In addition to this, the fwhm is greater than 90.6 mV, which is the expected value for an ideal one-electron redox process. Both of these observations can be attributed to repulsive interactions between neighboring redox sites, which becomes significant at a reasonably higher packing density of the monolayer,[27] and to rather slow electron-transfer reactions between the ruthenium and the platinum surface.[28] The relationship between the peak height and scan rate was not linear, as was expected for a redox-active species covalently attached on the electrode surface (diffusionless-controlled process), but rather showed a quadratic dependence.

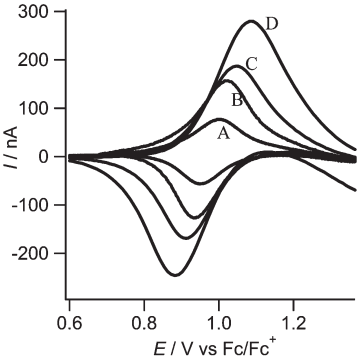

Figure 6. CV of Ru-SH adsorbed onto the platinum electrode recorded in an acetonitrile solution (0.1 M $TBAPF_6$) at different scan rates: (A) 100 mV s^{-1}; (B) 200 mV s^{-1}; (C) 500 mV s^{-1}; (D) 1 V s^{-1}.

Conductivity Measurements Using a Ga_2O_3/EGaIn Setup. In order to gain a better picture on how the electrons and holes can flow through the molecules, we formed tunneling junctions with SAMs of Ru-SAc. We formed SAMs of Ru-SAc on template-striped gold (Au^{TS}) bottom electrodes and used cone-shaped top electrodes of a liquid metal alloy of gallium and indium (Ga_2O_3/EGaIn)[15,16,29] to contact and to complete the tunneling junctions.[14] A surface layer of Ga_2O_3 on EGaIn readily forms under ambient conditions.[30] A schematic picture of the tunneling junctions is shown in Figure 7. In all experiments, we biased the Ga_2O_3/EGaIn top electrode and grounded the Au^{TS} electrode.

We used top electrodes Ga_2O_3/EGaIn for three reasons: (i) Junctions with top electrodes of Ga_2O_3/EGaIn are easy to assemble.[15] (ii) Junctions with top electrodes of Ga_2O_3/EGaIn have $J(V)$ characteristics that are dominated by the chemical structure of the SAM.[16] Thus, Ga_2O_3/EGaIn does not destroy the molecules in the SAM, unlike, for instance, direct metal deposition methods,[31] and the junctions are not dominated by artifacts, such as the formation and dissolution of filaments.[32] (iii) Junctions with top electrodes of Ga_2O_3/EGaIn are relatively mechanically stable.[16] This stability makes it possible to measure hundreds of $J(V)$ curves of single junctions and to collect statistically large numbers of data. Statistically large numbers of data have to be recorded and analyzed to discriminate the artifact from real data and to determine the reproducibility and yield of working devices.[16,33] Early work has shown that a liquid electrode, such as a

(24) Khalid, O. M.; Ku, S.-Y.; Wong, K.-T.; Bard, A. J. *Angew. Chem., Int. Ed.* **2009**, *48*, 9300–9303.
(25) Kalyanasundaram, K. *Coord. Chem. Rev.* **1982**, *46*, 159–244.
(26) Ricci, A.; Rolli, C.; Rothacher, S.; Baraldo, L.; Bonazzola, C.; Calvo, E.; Tognalli, N.; Fainstein, A. *J. Solid State Electrochem.* **2007**, *11*, 1511–1520.
(27) (a) Laviron, E.; Roullier, L. *J. Electroanal. Chem.* **1980**, *115*, 65–74. (b) Kondo, T.; Kanai, T.; Uosaki, K. *Langmuir* **2001**, *17*, 6317–6324.
(28) Laviron, E. *J. Electroanal. Chem.* **1979**, *101*, 19–28.
(29) Dickey, M. D.; Chiechi, R. C.; Larsen, R. J.; Weiss, E. A.; Weitz, D. A.; Whitesides, G. M. *Adv. Funct. Mater.* **2008**, *18*, 1097–1104.
(30) The thickness, composition, and surface roughness of the layer of Ga_2O_3 have been characterized. The electrical properties also have been characterized. The layer of Ga_2O_3 is about 2 orders of magnitude more resistive than bulk EGaIn, is about 1−2 nm thick, and is rough (the actual contact area is 20−40% of the measured contact area). We will report these findings in a separate paper.
(31) Walker, A. V.; Tighe, T. B.; Cabarcos, O. M.; Reinard, M. D.; Haynie, B. C.; Uppili, S.; Winograd, N.; Allara, D. L. *J. Am. Chem. Soc.* **2004**, *126*, 3954–3963.
(32) Beebe, J. M.; Kushmerick, J. G. *Appl. Phys. Lett.* **2007**, *90*, 083117–3.
(33) Kim, T. W.; Wang, G.; Lee, H.; Lee, T. *Nanotechnology* **2007**, *18*, 315204–8.

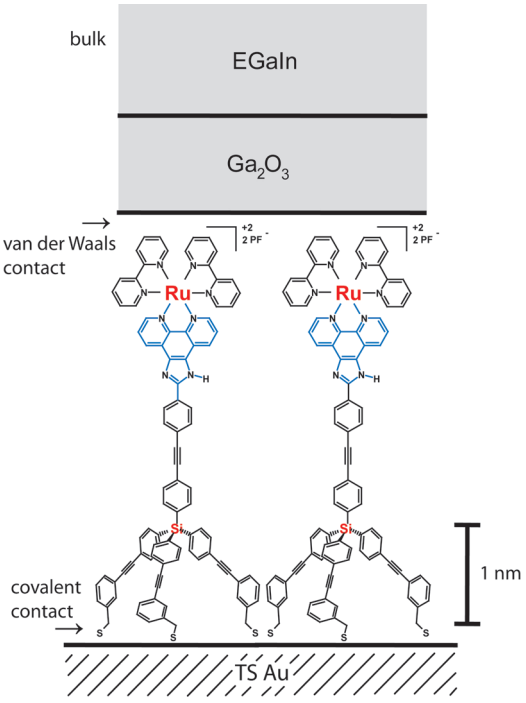

Figure 7. Schematic of the Au^{TS}-Ru-tripod//Ga_2O_3/EGaIn tunnel junctions. The EGaIn top electrode is biased, and the Au^{TS} bottom electrode is grounded.

mercury drop, could be the answer to measuring rather fragile monolayers.[34] However, the mechanical stability of the mercury-based junction is not so high, and indeed the use of this electrode is rather impractical for further developments. Junctions based on mercury-drop top electrodes only were stable, in best cases, up to 15 scans before the mercury top electrode amalgamates with the bottom electrode.[14] Ga_2O_3/EGaIn as a top electrode overcomes some of these problems and proved to be a possible answer in terms of stability and reproducibility.[15]

These junctions also have three uncertainties that are all related to the layer of Ga_2O_3. (i) The thickness of the layer of Ga_2O_3 is uncertain. We estimated the thickness of the layer of Ga_2O_3 to be 1−2 nm by time-of-flight secondary ion mass spectrometry and angle-resolved XPS. (ii) The electrical properties of the layer of Ga_2O_3 are uncertain. We estimated the resistivity of the layer of Ga_2O_3 to be about 2 orders of magnitude more resistive than that of bulk EGaIn but to be about 4 orders of magnitude less resistive than that of a SAM of $SC_{10}CH_3$.[16] Thus, we believe that the resistivity of the layer of Ga_2O_3 is negligible. (iii) The topography of the contact of Ga_2O_3 with the SAM is uncertain. We recorded optical micrographs of cone-shaped tips of Ga_2O_3 in contact with ITO. We estimated that the actual contact area is ~25% of the measured contact area.

The Ru-SAc monolayers were formed at the Au^{TS} electrodes for 24 h. The junctions were completed by contacting the monolayer with a conically shaped tip of Ga_2O_3/EGaIn. Typical junction sizes were 500−1000 μm^2. A total of 17 junctions were assembled at three different Au^{TS} surfaces. Of these 17 junctions, 14 were working and 3 were shorting; thus, the yield of the working devices was 82%.[35] The junctions were then scanned between −2 and +2 V as an example of a $J(V)$ curve. We performed a statistical analysis of the data by a procedure reported earlier.[16] The semilog plot of the average $|J|(V)$ curve is shown in Figure 8. The junctions were stable against these large potentials, and they could be measured for more than 1 h, obtaining 20−30 scans before they shorted or the experiments were stopped. We measured 60 traces per junction before we terminated the experiment. The relatively large stability and high yield in the working devices suggest that the tripod molecules are extremely stable and, most likely, constantly standing up and that the SAMs are densely packed.

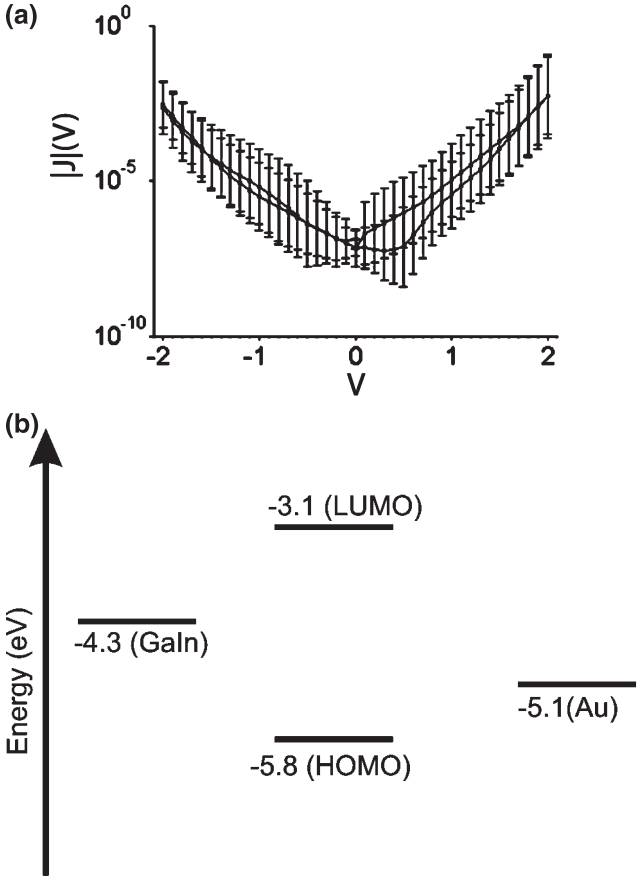

Figure 8. (top, a) Average $|J|(V)$ semilog plot of the TS Au−Ru//EGaIn junctions. One trace = 0 V → +2.0 V → −2.0 V → 0 V, and the arrows indicate the scan direction. (bottom, b). Energy levels of the Ru-SH molecule and the electrodes in a EGaIn setup at an open circuit with respect to a vacuum.[36]

The Ru-tripod has accessible HOMO and LUMO levels, which may come in resonance with the Fermi levels of the electrodes at large bias. The tripod molecule studied in this paper is a highly conjugated molecule; thus, the HOMO and LUMO orbitals will, to a certain degree, be delocalized. Given the length of the molecule, it is fair to assume that both the HOMO and LUMO will be located unsymmetrically inside the junction. For this reason, they are, in principle, unsymmetrically coupled to the electrodes and should be coupled more strongly to the Ga_2O_3/EGaIn top electrode. We believe that the HOMO and

(34) Tran, E.; Rampi, M. A.; Whitesides, G. M. *Angew. Chem., Int. Ed.* **2004**, *43*, 3835–3839.

(35) Because the sizes of the AFM tip and EGaIn droplet are not comparable and are roughly 3 orders of magnitude apart, an uneven surface on the nanoscale does not necessarily mean a macroscopic effect because the area measured under EGaIn is several micrometers while the defect measured with AFM is on the order of a tenth of a nanometer. The measurements are highly reproducible, and the scan can be repeated several times without any degradation or destruction of the layer, indicating a very stable surface.

LUMO levels are unsymmetrically coupled to the bottom and top electrodes, but the presence of mobile PF_6^- anions in the junction will, at least partially, compensate for that. The presence of mobile PF_6^- anions in the junctions may cause large potential drops at the tripod//Au interface, facilitating the hole-injection process.

Figure 8 shows the approximate energy diagram. The HOMO and LUMO levels were estimated by electrochemistry data[36] and found to be −5.8 and −3.1 eV, respectively. Ga_2O_3/EGaIn has a work function of ∼−4.3 eV and gold of −5.1 eV. We do not know the details of the mechanism of charge transport, but we hypothesize that charge can be injected in the HOMO and LUMO levels of the molecules. Currently, we are investigating tripod molecules with different metal centers and ligands, hence different HOMO and LUMO levels, to gain more insight into the tunneling processes across these junctions. Furthermore, as a possible extension of this work, the great stability of the TS Au/Ru-tripod//EGaIn tunnel junctions could lead to investigations of the charge-transfer processes of electroluminescent molecules in tunnel junctions (single-layer electroluminescence).

Conclusions

We have prepared and investigated a series of ruthenium complexes, two of them containing a tripod system. The tripod can be further chemically functionalized with thiol groups for its attachment to metallic surfaces through more thiols to stabilize the binding and allow a perfect perpendicular geometry of the system. The structure of the complexes has been, in fact, designed in a way that the ruthenium center is coordinated to two bipyridine ligands and a chelating phenanthroline bearing a five-membered ring for its axial functionalization. This approach allows the complexes to be luminescent and, for the thiol derivative, to stand almost vertically when assembled to a surface. We have demonstrated that the gold surface quenches the emission of the ruthenium complexes self-assembled on the metal surface. The SAMs of ruthenium complexes have been employed to construct a redox-active junction to investigate the conductivity of the assembled molecules on the gold surface by using an EGaIn eutectic as a second electrode. The results showed that the monolayers are stable and a rectification behavior is observed. In view of the fact that the complexes are also electroluminescent, an understanding of the charge injection and transport could lead to important consequences for the design of LEEC and other electroluminescent devices.

Acknowledgment. Funding from NanoNed (Project AMM7010), which is an initiative from the Dutch ministry of economic affairs, is acknowledged. The authors acknowledge Dr. Federico Polo (Westfälische Wilhelms-Universität Münster) for helpful discussions.

Supporting Information Available: Excitation spectrum of a Ru-SAc monolayer on a gold substrate (Figure S1), XPS spectrum of Ru-SH bound to a gold substrate (Figure S2), statistical analysis of the data from tunneling junctions (Figure S3), and estimation of the surface coverage. This material is available free of charge via the Internet at http://pubs.acs.org.

(36) Bard, A. J.; Faulkner, L. R. *Electrochemical Methods—Fundamentals and Applications*; John Wiley & Sons: New York, 2001.